

## ADVANCES IN MODELING THE UNIVERSITY OF MARYLAND ELECTRON RING\*

R.A. Kishek<sup>#</sup>, M. Cornacchia, K. Fiuza, B.L. Beaudoin, S. Bernal, I. Haber, T. Koeth, P.G. O’Shea, D.F. Sutter, and H. Zhang, IREAP, University of Maryland, College Park, MD 20742, U.S.A.

### Abstract

The University of Maryland Electron Ring (UMER) [1] is a research accelerator designed to operate with extreme space charge. Recent high-precision experimental measurements of tune, dispersion, chromaticity, response matrix elements, and other parameters [2-4] have prompted a refinement of the models used to describe the machine. Due to the low energy (10 keV) of the electrons, the dipole and quadrupole magnets used are air-core printed-circuit coils whose fields we calculate using a Biot-Savart solver. Different levels of approximations for the magnetic fields have been developed. The simple models are compared against simulations using the particle-in-cell code WARP [5], the accelerator code, Elegant [6], as well as experiments. The improved modeling has significantly reduced the discrepancies between simulation and experiment.

### INTRODUCTION

High beam quality, described by a dense, compact phase space, is critical for many modern accelerator applications. The University of Maryland Electron Ring (UMER) [1] is a small storage ring dedicated to research on beams at the intensity frontier. The low electron energy (10 keV), relatively high current (0.5-100 mA), and low rms emittance (0.3-3  $\mu\text{m}$ , normalized) contribute to significant space charge forces that dominate the beam dynamics. The simulation models previously used to describe the UMER lattice were successful in modeling first-turn experiments (e.g., Refs. [7, 8]). Studies of beam physics over longer propagation distances, however (e.g., to investigate resonances), require a higher level of accuracy.

Recent high-precision experimental measurements of tune, dispersion, chromaticity, and other parameters (Sec. 3.4) [2-4] have therefore prompted a refinement of these models. For example, simple calculations of tune have differed by as much as 0.5 from the measured values. The discrepancy arose from uncertainties in modeling the bending dipoles and the injection “Y-section”. We have therefore reexamined the magnet models in detail in order to understand how to better represent the lattice.

To validate the models, we have devised a method for extracting the focal lengths of the magnets from response matrix measurements. This is discussed at length as it is of general interest. We also compare different levels of approximation of the lattice models using the codes

WARP [5] and Elegant [6]. The improved modeling has significantly reduced the discrepancies between simulation and experiment.

### UMER MAGNET MODELS

Due to the low beam energy, the dipole and quadrupole magnets used in UMER are air-core printed-circuit coils in which the fringe fields are dominant [9-10]. These magnets were carefully designed to minimize the integrated nonlinearities. For beam dynamics calculations, different levels of approximations for the magnetic fields have been developed. The most detailed calculate the fields using a Biot-Savart solver on an arbitrarily-fine grid, which can then be used in WARP. It is also desirable to derive simpler models, for example to use with TRACE3d for beam matching. For the ring quadrupoles, we have extensively compared different models and found that a hard-edge model suffices for accurate calculations. The dipoles, however, are more problematic, because the beam trajectories can deviate substantially from the nominal, particularly due to modifications to the closed-orbit from the Earth’s magnetic field. For example, Figure 1 illustrates the effects of neglecting the dipole and/or the Earth field on the beam envelope.

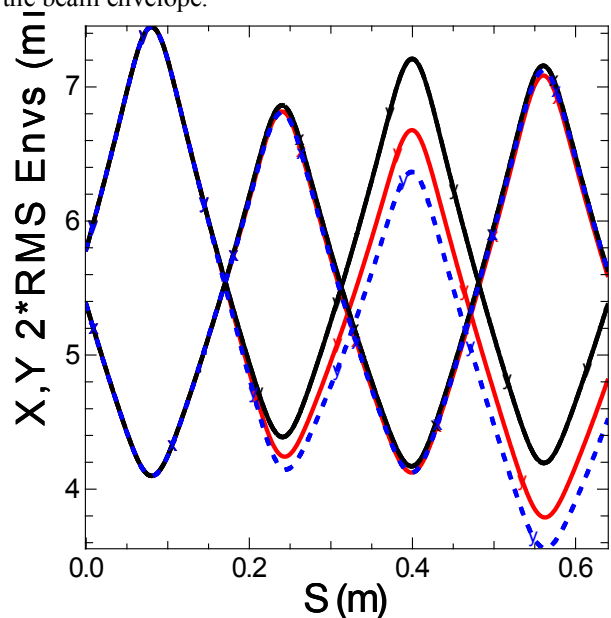


Figure 1: Effect of dipole and Earth field on envelope of a 23 mA beam in two FODO periods: quadrupoles only (black dashed); dipole added but no Earth field (blue dotted); with both dipole and a 0.4 G vertical Earth field (red solid). In the last case, the dipole strength is adjusted to compensate for the Earth field.

\*Work supported by US Dept. of Energy Offices of High Energy Physics and Fusion Energy Sciences, and by the Office of Naval Research and the Joint Technology Office.

<sup>#</sup> ramiak@umd.edu

We have found it possible to model the dipole as a thin lens and still obtain good predictions of tune values, but the focusing terms in the dipoles must be calculated properly. The largest contribution to the gradient is edge focusing, which manifests in the vertical plane, but is cancelled in the horizontal plane by the geometric focusing [11]. In addition, there is a smaller contribution due to the sextupole term and the horizontally curved trajectory in a straight-edge dipole. Although, by design, the sextupole component disappears when integrated along the dipole axis, a beam moving along the curved reference trajectory will experience a gradient. We have quantified this effect by fitting polynomials to the radial profile of  $B_y$  to obtain the sextupole term  $S(s)$ , from which we then estimate the horizontal focusing gradient using the relation  $g_x(s) = 2S(s)x(s)$ . The vertical integrated gradient is obtained directly from the polynomial fit to  $B_{\perp}$  (defined as the normal in the horizontal plane to the reference trajectory through the dipole). From the integrated gradients, we obtain the focal lengths:

$$\frac{1}{f} = \frac{\int g ds}{[B\rho]} \quad (1)$$

Note that in order to compensate for the Earth field, the dipole strength is adjusted to maintain the same average bending angle per section, and the dipole focusing is accordingly reduced.

## EXPERIMENTAL AND NUMERICAL VALIDATION

We have validated this model in two ways. First, we used the WARP code to integrate particle orbits using the detailed first-principles field descriptions. Second, we derived the focal length from experimental measurements of the response matrix in the first turn of the ring, where the lattice is periodic and the measurement is not complicated by traversal of the injection Y section.

The simulation test (using the WARP-XY slice code) involved running narrow lines of parallel particles with zero divergence, low current ( $10^{-9}$  A), and miniscule emittance ( $10^{-15}$ ) through the different magnets to test their focusing effects. It was found that a step of 0.25 mm was needed to resolve the fringe fields. The most detailed model tested was a gridded field with 0.5 mm resolution generated from the full double-layer spiral geometry of the dipole. This was only slightly more accurate than a simpler single layer of loops instead of spirals, the two differing by only 0.02% in the gradients. To verify the WARP bending algorithm, we additionally tested a sector dipole and a box dipole, both of which behaved as expected from theory.

Figure 2 illustrates the trace space before and after passage through the dipole. The focal length associated with dipole focusing is measured directly from the rotation of the phase space.

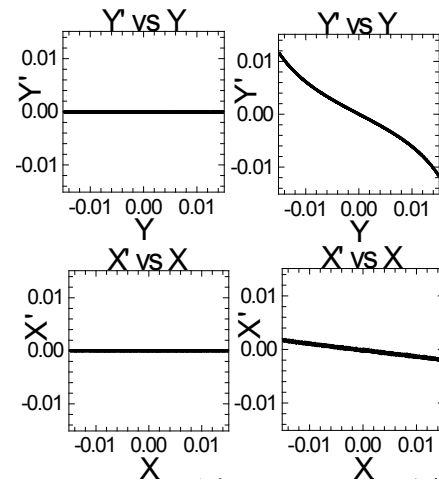


Figure 2: Trace space plots before entry (left) and after exit (right) from the double-layer spiral dipole. Initial particle distribution has large size in Y to test vertical focusing (top), and in X to test horizontal focusing (bottom).

Measuring the dipole focusing from experiment is more involved. We rely on a method for measuring the lattice phase advance from response matrix data, similar to Ref. [12]. We analyze the data differently, however, in order to minimize the effects of spurious data points caused by distribution of ambient magnetic fields, BPM errors, and other local errors. For each dipole-BPM pair, we gather position data for seven different dipole settings. The slope of the linear fit is the response matrix element. Dipole settings for which the centroid is measured further than 5 mm from the pipe axis are thrown away to improve the linearity of the fit. Rather than include all the response matrix elements in the phase advance calculation, we reduce the data in each diagonal to the median of that diagonal (Figure 3). This ensures that spurious data points do not affect the calculation and ignores cell to cell variations.

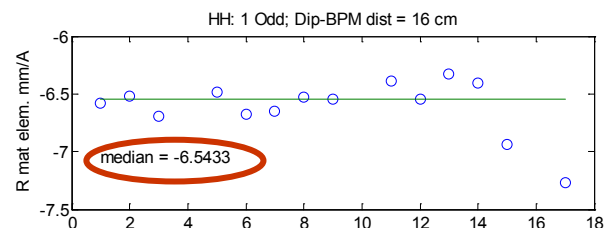


Figure 3: Horizontal 1st-turn response matrix elements (in mm/A) along the main diagonal, corresponding to dipoles 16 cm upstream of BPMs. The median method eliminates the effect of incorrect calibration of the last two BPMs.

Next, the medians of each diagonal are plotted as a function of the distance between dipoles and BPMs for that diagonal (Figure 4). This essentially samples a betatron oscillation. To this we fit a sinusoid, the frequency of which corresponds to the lowest-order Fourier component of the sampled betatron oscillation.

The phase advance is then calculated from  $\sigma_e = kS_0$ , where  $S_0 = 0.32$  m is the lattice period and  $k$  the wavenumber obtained from the fit.

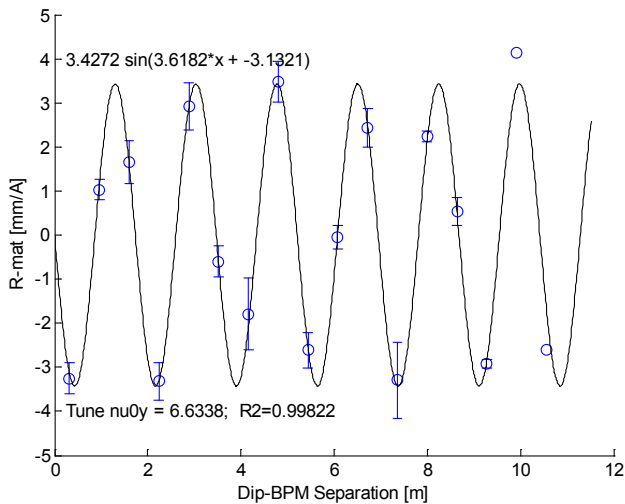


Figure 4: Vertical response matrix diagonal medians as a function of dipole/BPM distance. The phase advance can be obtained from the frequency of the sinusoidal fit. In fitting, we ignore the last 4 data points corresponding to the shortest diagonals, whose values are skewed by the faulty calibration of the last two BPMs.

The phase advance measured by this method includes the effect of image forces. To get the zero-current phase advance, the value must be corrected using [13]:

$$\sigma_o = \sqrt{\sigma_e^2 + \frac{KS^2}{b^2}}, \tag{2}$$

where  $K$  is the generalized perveance and  $b$  the pipe radius.

The focal length of the dipole is calculated by considering the transfer matrix of a cell consisting of two quadrupoles whose strength is known and a dipole as a thin lens of focal length  $f$ . The latter is derived from the measured phase advance:

$$f = \frac{M_{12}}{\text{Tr}[M] - 2 \cos \sigma_o}, \tag{3}$$

where  $M$  is the transfer of the FODO cell without the dipole.

Comparing the dipole focal lengths obtained by the different methods, Table 1 shows good agreement between the first-principles calculation from the integrated gradient and the WARP simulation. The experimental data shows somewhat stronger dipole focusing, especially in the horizontal direction. We expect that the recent installation of new printed circuit quadrupoles, the improved quality of the response matrix data due to repair of some BPMs, as well as better

steering optimization, will reduce the experimental uncertainty.

Table 1. Inverse focal lengths of the ring dipoles ( $1/f$ , units:  $m^{-1}$ ) from first-principles theory, WARP, and values derived from response matrix experiments, for a bend angle of  $10^\circ$  (no Earth field) or  $7.8^\circ$  (with Earth field).

	No Earth Field		Vertical Earth Field = 0.4 G	
	y	x	y	x
<b>Theory</b>	0.495	0.129	0.386	0.101
<b>WARP Simulation</b>	0.566	0.133	0.333	0.10
<b>Experiment Fit</b>			$0.46 \pm 0.1$	$0.20 \pm 0.1$

### CONCLUSION

We have demonstrated a procedure for analyzing the focusing from air-core dipole magnets from first-principles. The derived focal lengths are systematically compared against WARP simulations and experimental data. We have also shown a systematic procedure for measuring the phase advance and dipole focal lengths from response matrix experiments. The improved modeling of the UMER dipoles has succeeded in reducing the tune discrepancies between calculation and experiment to within 0.1. We are currently applying a similar approach towards reducing the uncertainties in modeling the Y-section injection magnets, consisting of a pulsed dipole and oversized, pulsed quadrupoles, one of which is significantly offset from the reference beamline.

### REFERENCES

- [1] T.F. Koeth *et al.*, these Proceedings (2011).
- [2] D.F. Sutter *et al.*, Proc. PAC 2009, ID: FR5PFP063.
- [3] C. Wu *et al.*, Proc. PAC 2009, ID: FR5REP029.
- [4] S. Bernal *et al.*, Proc. AAC 2010, p.580.
- [5] D.P. Grote *et al.*, NIM A **415**, 428 (1998).
- [6] M. Borland, APS Tech. Note LS-207, September 2000.
- [7] R.A. Kishek, S. Bernal, C.L. Bohn *et al.*, " Physics of Plasmas **10** (5), 2016 (2003).
- [8] D. Stratakis, R.A. Kishek, I. Haber, S. Bernal, M. Reiser, and P.G. O'Shea, *PRST:AB* **12**, 064201 (2009).
- [9] T. F. Godlove, S. Bernal, and M. Reiser, Proc. PAC 1995, 2117 (1995).
- [10] W.W. Zhang, S. Bernal, H. Li *et al.*, *PRST:AB* **3**, 122401 (2000).
- [11] Philip J. Bryant and Kjell Johnsen, *The Principles of Circular Accelerators and Storage Rings* (Cambridge: Cambridge University Press, 1993), Sec. 3.3.2.
- [12] Chung, Decker, and Evans, Proc. PAC 1993, p. 188.
- [13] Martin Reiser, *Theory and Design of Charged Particle Beams*, 2<sup>nd</sup> ed., (Wiley, V.C.H., 2008), Eqn. 4.238a.